CHAPTER 11

Tides at a coast

Jennifer M. Brown, Angela Hibbert, Lucy M. Bricheno, Elizabeth Bradshaw, and Amani E. Becker
National Oceanography Centre, Liverpool, United Kingdom

1. Introduction

The tides through time discussion in Section II of this book focuses on the big picture, so we will open part III by looking at smaller scales. As a reminder to the reader, basic tidal theory is described in Chapter 4, so we will kick off with a chapter on tides at coastlines and the effects tides have on the transport of sediment and other matter. We will also explore the wide ranges in tides encountered at the coast and how the tide shapes our environment.

2. Tides at the coast

Tidal waves form in the open ocean but are modified by their interaction with the coast. If the globe was entirely covered in water, tides would track the progression of the Sun and the Moon relative to the Earth. Due to the finite depth of the ocean, the speed of the tidal wave is constrained. The tidal wave is modified by the interaction with shallow bathymetry and coastlines. There is a large variation of tidal range around the world. Some of the largest tidal ranges are found in Alaska and in the Bay of Fundy, Canada, and in comparison, there is little discernible tide in the Baltic and Mediterranean seas (Pugh and Woodworth, 2014).

The pattern of the tide can be diurnal (one high and one low water a day), semi-diurnal (two high and low waters per day), or mixed (where some days the tides are diurnal and other days they are semi-diurnal, varying from spring to neap tides throughout the month). Co-tidal lines on charts show the progression of the tidal wave in a given area and connect sites that experience points in the tidal cycle simultaneously. They also show areas of zero tidal amplitude, called amphidromic points. Tidal charts also show co-range lines, connecting points of equal tidal range (e.g., Fig. 11.1).

https://doi.org/10.1016/B978-0-323-90851-1.00019-4

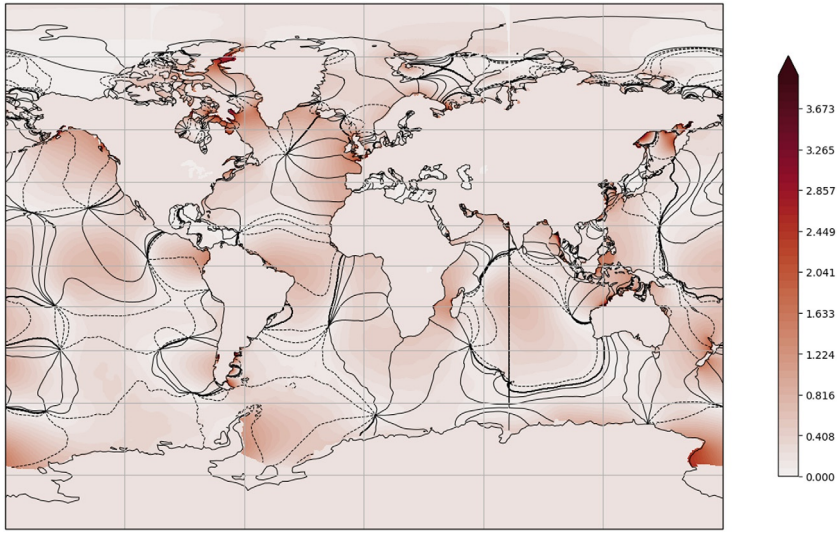

Fig. 11.1 A co-tidal chart of M_2 tidal range (m) in the global seas showing amphidromic points (Byrne et al., 2021). These data are from a global tide model.

In general, the dominant tidal constituent is the semidiurnal lunar tidal component M_2, which has a 12-h 25-min period. As the tide travels along the coast, when the wave meets the coastline in shallow water, it is distorted and the tidal wave becomes asymmetric. The movement at the coast creates shallow water constituents (as described later in this section). Tidal distortion is often seen with propagation up estuary or into a delta, see for example Fig. 11.2.

Chapter 4, Section 4.5 (The real world) provides a detailed description of how the tidal wave is modified by the depth of the ocean and how ocean basins can set up resonance.

The tidal wave can further be constrained by coastal geometry and local morphology. Shallow water tides (see Table 4.4 in Pugh and Woodworth (2014) for a list of examples) can reach large amplitudes, resulting in strong tidal distortion. Tidal distortion is caused by nonlinear interaction of the individual major tidal components. It can be caused by the effects of shallow water in the inertial term (acceleration due to external pressure gradient, which drives the tidal wave propagation), the advective term (usually negligible) or the friction term for example, Prandle (2003). The offshore tide becomes strongly distorted as it propagates into shallow water and estuarine systems. As the tidal wave becomes distorted, more energy moves from the

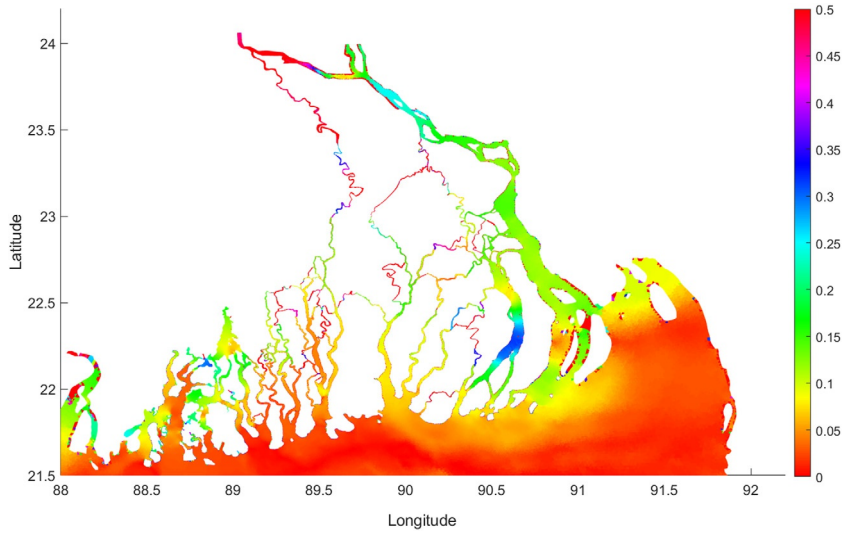

Fig. 11.2 Tidal distortion (ratio M_4 amplitude/M_2 amplitude) modeled during March through the Ganges-Brahmaputra-Meghna Delta.

major constituent M_2 into the higher frequency M_4 constituent (and other higher harmonics like M_6). Tidal distortion can evolve throughout the year, due to seasonal morphological and hydrological changes (caused by tide-river interactions—see Section 3.2). In regions of very large seasonal variation in river discharge the wetting and drying of river channels cause major morphological changes. This can modify tidal hydrodynamics in inter-tidal areas by changing areas of frictional dissipation.

3. Tidal interactions with other physical processes

Where tides interact with other physical properties (i.e., as combined hazards), they can cause damage to property and infrastructure such as roads, railways and that associated with energy generation and supply. Damage may be due to flooding during especially high tides (sometimes called "King tides"), and erosion or other physical damage may be caused by waves brought further inland during a high tide. High tide flooding (sometimes referred to as "nuisance" or "passive" flooding) has a range of impacts such as road closures, train delays and cancelation, overwhelmed drainage systems, and deterioration of coastal transport infrastructure. The incidence of high tide flooding is increasing due to sea-level rise, land subsidence, and with the loss of natural coastal barriers. It is a particular problem for

islands, especially coral atolls (Esteban et al., 2019), but also effects continental coasts, for example the east coast of North America (Ray and Foster, 2016).

When high tides occur simultaneously with a storm surge, during hurricanes and violent storms, the result can be extreme water levels. The damage caused to coastal communities and infrastructure by these events is well documented: examples include storm surges generated by Hurricane Katrina in New Orleans during 2005, storm Xaver impacting the North Sea and Humber estuary (UK) in 2013, and Hurricanes Maria and Irma in the Caribbean during 2017. Coastal features, such as estuaries, may increase the magnitude of these events (Lyddon et al., 2018), causing increased flood risk.

Seiches are high frequency oscillations, analogous to water sloshing in a bath, that can greatly alter the tide and cause considerable damage to property (Pugh et al., 2020). The waves can be tens of centimeters in amplitude and in the Mediterranean, seiching (known locally as the Rissaga) in Minorca, has been known to cause damage to shipping. The fundamental frequency is proportional to $1/\sqrt{h}$, where h is the water depth. The water body in a basin, harbor or bay resonates after being forced by strong winds, changes in air pressure or by the tide itself. Seiches can also be triggered by seismic activity and landslides. Waves also interact with the tide (Section 3.3), with wave height increasing at high tide in some locations (Lewis et al., 2019). Large waves at high tide may overtop coastal defenses, erode natural defenses and damage infrastructure.

Other sea-level hazards that may interact with tides include tsunamis and meteotsunamis. Tsunamis are generated by events such as submarine earthquakes, underwater landslides and volcanic eruptions, which displace large volumes of water. Equilibrium is restored through the propagation of long ocean waves, whose speed is dependent upon ocean depth. As a result, in deep water, tsunamis travel quickly and have small amplitudes, but on reaching shallower depths, they slow and the wave crest rises, sometimes attaining amplitudes of tens of meters, which is why they pose such a danger at the coast. Energetic events, such as the 2004 Sumatra tsunami which killed over 200,000 people, can travel around the world. Meteotsunamis are also long ocean waves, with behavior similar to tsunamis, but are generated by atmospheric forcing (Vilibić et al., 2021). The waves have a frequency of minutes to hours. A meteotsunami can form over several minutes to hours, when severe weather systems (e.g., thunderstorms, atmospheric gravity waves, and rapid jumps in air pressure) interact with the coastline where local resonances can occur, and they can be particularly destructive to coastal habitats.

The relative risk at the coast from marine hazards can be quantitatively assessed using a combined vulnerability index (CBVI), as demonstrated for the Caribbean Sea by Jevrejeva et al. (2020). A CBVI includes the external effects of tides, waves, sea level, and storm winds to calculate the exposure at the coast to these physical factors and provides evidence for coastal resilience planning.

3.1 Tidal interaction with the atmosphere at the coast

The tidal cycle can be modified by interaction with the atmosphere. A storm surge is the difference between the observed sea-level height and the predicted height caused by changes in atmospheric pressure and wind piling up water at the coast. When a storm surge coincides with high tide, it can lead to coastal inundation and cause considerable damage (see Section 6.3 for further explanation).

The skew surge is the difference between the maximum observed and maximum predicted sea-level height during the tidal cycle, the former not necessarily occurring at the time of predicted high water (Pugh and Woodworth, 2014). Skew surge is an important indicator for monitoring hazards at the coast as it gives a realistic representation of the magnitude of the surge component.

The meteotsunamis mentioned above are another example of ocean-atmosphere interactions that can be destructive to coastal habitats.

3.2 Tidal interaction with regions of freshwater

Freshwater can play an influencing role on the behavior of tides in deltas, estuaries, and at river mouths, which all experience large freshwater discharge. 'Regions of freshwater influence' or ROFIs (Simpson et al., 1991), are a catch-all description of these areas. At the coast and in shallow areas, seasonal river discharge can change the water levels considerably. This can affect the tidal dynamics, by altering the bottom friction and water depth, and generating asymmetries in the tidal wave. The presence of density driven circulations at slack tide can also alter the tidally averaged (net) circulation (Brown et al., 2014). River-tide interaction is one of the questions of common concern in tidally dominant estuaries, see for example Horrevoets et al. (2004), Sassi and Hoitink (2013), Leonardi et al. (2015), and Hoitink and Jay (2016). Once the tidal wave propagates upriver, the modulation of tidal amplitudes at specific tidal frequencies happens due to the damping induced by bottom friction, but also the blocking of the tide

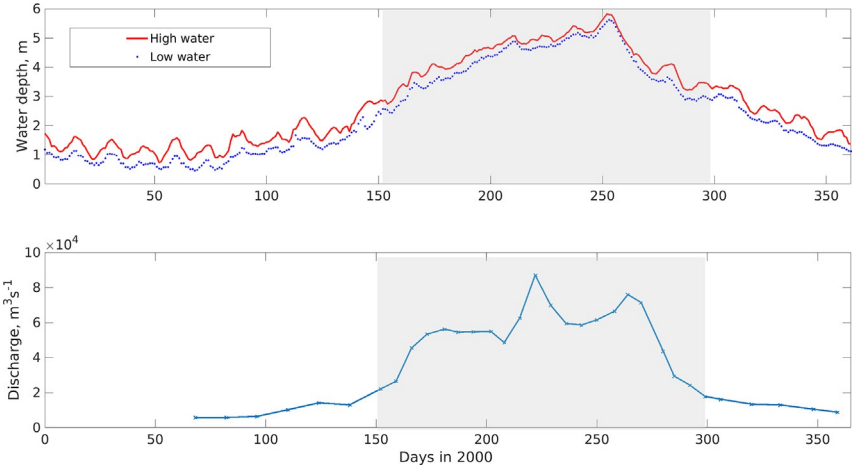

Fig. 11.3 Time series of high and low tides observed at Sureswar, Bangladesh, on the river Ganges, (top), and co-located river discharge measurements (below), with the wet season shaded in gray.

due to the freshwater outflow, which can also cause the displacement of the mean water level (Godin, 1999).

Fig. 11.3 shows an example time series of tidal levels and river discharge observed at Sureswar, Bangladesh on the river Ganges (model defined in Bricheno et al., 2016). During the seasonal monsoon, the river discharge can vary enormously (by more than 2 orders of magnitude, from about 5000 to over 100,000 m^3/s). The addition of this volume of freshwater has a big impact on the water levels, and thus the hydrodynamics in the river and estuarine channels. Note how at the height of the monsoon the tidal range is suppressed by the river water flowing offshore. Compare this with the dry season, when the daily tidal range and spring-neap range is larger, as the tidal energy can penetrate further inland. As well as modulating the water level, freshwater, and large river discharges can change tidal currents and the transit of the tidal wave. Fast offshore currents generated by river flow can delay the arrival of the high tide, as well as suppressing the tidal range by retarding the speed of the tidal wave.

3.3 Tidal interactions with wind generated sea surface waves at the coast

Waves on the sea surface at the coast can be generated by local winds and/or the result of surface wind waves that have propagated toward land, as swell, from distant storms. Like meteorological influences (wind and pressure) and

freshwater inflows, surface wind waves also contribute to coastal circulation and water levels. The generation of radiation stresses that are created during wave shoaling and breaking, in estuaries and at the open coast, cause wave-driven circulations and wave set-up (Longuet-Higgins, 1970a,b; Longuet-Higgins and Stewart, 1964). The coastline geometry plays an important role in controlling the magnitude of the surface wind waves and can thus influence the local flood and erosion hazard (Xie et al., 2019). During storm conditions the gradients in radiation stress will result in different water levels than predicted for the tide alone (Idier et al., 2019). Modification of the residual circulation (and enhanced resuspension processes, Green and Coco, 2014) during storm wave conditions in turn influences the transport of suspended or dissolved material, sometimes counteracting the net transport pathways due to the tide alone (e.g., Brown and Davies, 2009). Nearshore current observations made at Sea Palling, East Anglia UK, have shown that during a storm the wave driven nearshore current can temporarily prevent the normal reversal of the tide (Bell, 2010). Surface wind waves can also influence the circulation through: wave-enhanced stress (and turbulence) at the surface and near bed, and Stokes' drift.

Sea surface wind waves are sensitive to changes in depth and current (Wolf and Prandle, 1999). Tides (like other coastal circulation processes) influence surface wind wave propagation by causing wave refraction, a Doppler shift of the wave period, and modify the frictional influences due to bottom stress and current shear in shallow water. Low tidal levels, noticeably reducing depth, and fast currents in shallow water can increase surface wind wave dissipation. The tidal time-variation in water depth and current velocity often creates a clear modulation of the wave height, which often matches the dominant tidal period (Fig. 11.4). Surface wind wave and tidal interactions can in turn impact other processes such as sediment transport, due to the timing of wave-enhanced bottom stress relative to the net circulation at that time. In shallow water, the understanding of wave-circulation interactions are therefore critical to determine the net transport of properties over different time periods as the instantaneous and cumulative impact of calm and stormy conditions shape our shorelines and flushing times of coastal waters. Understanding the long-term interaction of tidal and wave driven circulation is therefore critical for the effective management of beaches and coasts.

To better understand the interactions between tides and waves, numerical models are often used to isolate (turn on and off) processes to assess their contribution to the prevailing conditions (see Ardhuin et al., 2012; Bolaños

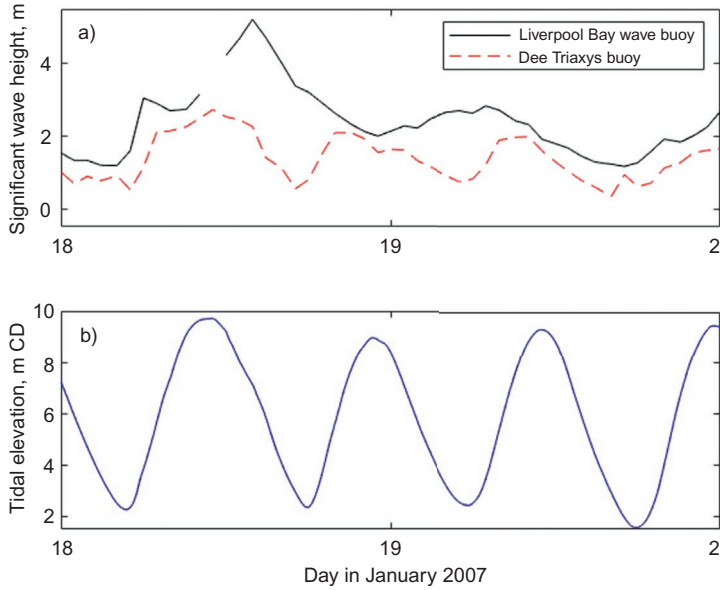

Fig. 11.4 (A) Significant surface wind wave heights observed in January 2007 by the operational Liverpool Bay wave buoy (part of the national WaveNet program) and temporary wave buoy deployment in the Hilbre channel close to the mouth of the Dee estuary (run by the National Oceanography Centre). (B) Tide gauge data from the nearby Liverpool Gladstone Dock.

et al., 2011). To simulate the wave-circulation interactions across a region requires a spectral (2-dimenstional) wave model to be coupled to an ocean circulation model, and both models to be forced with the same meteorological conditions. While 2-dimensional (depth-averaged) hydrodynamic models are more efficient and considered to be suitable for wave and water level hazard impact studies, 3-dimentional hydrodynamic models may be required in locations of complex bathymetries (e.g., estuaries and deltas) to accurately represent the depth to which the surface wind wave oscillations penetrate. The Dee estuary in the North West of England, where the mean spring tidal range exceeds 8 m, is an example of a site where the modeled surface wind wave field is sensitive to the vertical and temporal variability in the circulation. In turn the (weaker) cross-channel circulation is modified by the feedback from the radiation stress (Bolaños et al., 2014). Due to the large tidal range in the eastern Irish Sea, there have been numerous studies in this area investigating wave-circulation interactions (e.g., Brown and Wolf, 2009; Lewis et al., 2019). Fig. 11.4 shows the surface wind wave heights measured offshore in Liverpool Bay and concurrently in the nearby Dee

estuary. This figure illustrates the M_2 tidal modulation of the surface wind wave height in shallower water. Lewis et al. (2019) found surface wind wave heights in the Irish Sea could be up to 20% larger in some regions at high tide due to wave-tide interaction. This has important implications for coastal flood hazard and energy generation (e.g., Lewis et al., 2014, 2019).

Other studies have found the effect of wave-current interaction in shallow seas such as the Southern North Sea can change wave height by about 3% and wave period by more than 20% (Osuna and Monbaliu, 2004). Such findings have implications for shipping, fisheries, and particularly marine renewable energy. Observations have shown tides can modulate wave power (Davidson et al., 2008), while high wave conditions can reduce the amplitude of the tidal current (Wolf and Prandle, 1999).

Understanding the interactions between waves and tides is vital for coastal flood and erosion hazard management. Tides control the movement of the surf zone across the intertidal zone and the breaker position relative to flood defenses. At the shoreline surface wind waves will either dissipate, reflect or partially reflect as they run-up over the beach profile and interact with any existing structures (Scott et al., 2011). During a period around high tide, wave impact can cause the overtopping of coastal structures or the overwash and/or erosion of natural defenses, such as sand dunes and gravel barriers. Where tidal ranges are smaller, waves may pose a hazard at all stages of the tide. Fig. 11.5 illustrates wave overtopping of a sea wall in a hypertidal regime, that is, a spring tidal range greater than 6 m. In this example, the overtopping is restricted to approximately two hours around high water and is asymmetric around that time, with flood dominance in the duration and magnitude of the overtopping. The underlying coastal bathymetry and beach profile has a critical role to play in refraction of the waves. The direction and magnitude of any current is also important. Focusing of the waves due to depth and current refraction can make locations vulnerable or create a tidal asymmetry in coastal wave hazard.

Knowing the combinations and interactions of tides with other ocean and meteorological conditions that pose a threat to coastal habitats, communities, industry, and infrastructure is critical for the preparation of hazard response plans and the construction of early warning systems. Very often numerical approaches are used to explore the sensitivity of the system and the impact of uncertainty in our assumptions/understanding (e.g., Zou et al., 2013). To manage coastal hazard and understand hazard impacts, the annual probability of conditions occurring is often used. The joint probability of surface wind waves and high water levels occurring together is used

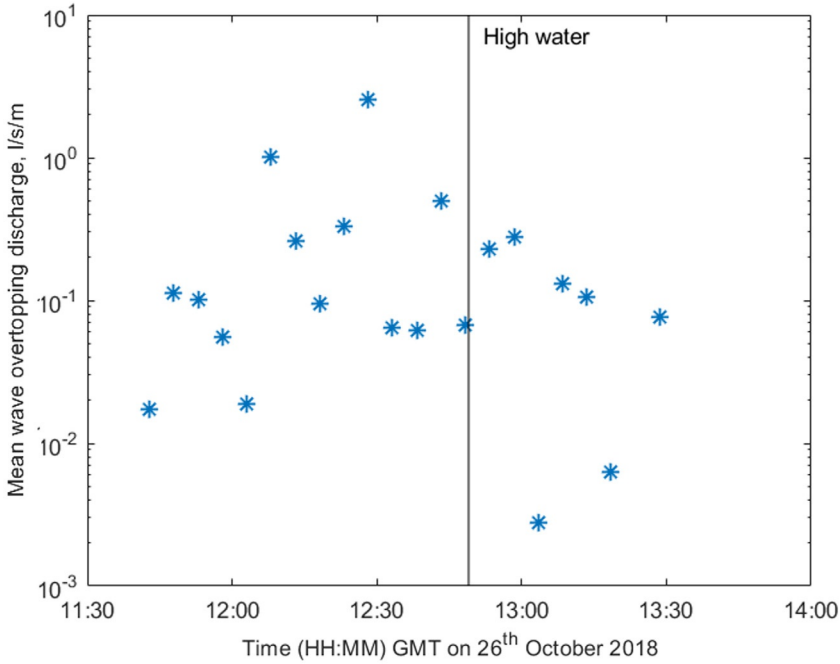

Fig. 11.5 Wave overtopping discharge at Crosby (North West England) measured on a wave-by-wave basis and averaged over a 5-min processing window (Brown et al., 2020). The data are plotted at the center of the processing window and represent the conditions when wave spray passes the hand railing approximately 30 cm inland of the crest of the sea wall. The offshore wave height was 2.3 m at high tide and the tidal range that day was 8.2 m.

as a way to categories the severity of the coastal conditions (e.g., Wadey et al., 2015), while multivariate analysis (e.g., Gouldby et al., 2017) is considered to be a more sophisticated approach to determine the probability of hazard impact taking into consideration other factors like the local wind influence on structure overtopping. Such an approach can be used for both hard engineered (e.g., Salvadori et al., 2015) and natural (e.g., Corbella and Stretch, 2012) shorelines.

4. Transport of matter

The movement of the tide leads to all manner of transports. Tides can move around particulate and dissolved biogeochemical tracers and physical properties, including (for example) heat, freshwater, nutrients, carbon, oxygen, fish larvae, sediment, and pollutants. The major impact of the tide at the

coast is the movement of seawater inland, in estuaries and deltas, and the vertical mixing of properties through the water column. Tides are a key source of kinetic energy that transport matter and generate turbulent mixing in shelf seas. The speed and trajectory at which matter is transported will depend on its height within the water column, which may change with time due to vertical mixing and the resuspension and settling of material. Characterization of the tidal velocity profile and energy dissipation is not only critical for understanding the transport of material, but also for the effective progression of the tidal-stream energy industry (Lewis et al., 2017). Due to process interactions and the generation of asymmetries in shelf seas, net circulation can occur over different time scales (e.g., a tidal cycle, a storm event or seasonal and annual time scales). Fig. 11.6 illustrates the net circulation over an extended period around the southern North Sea.

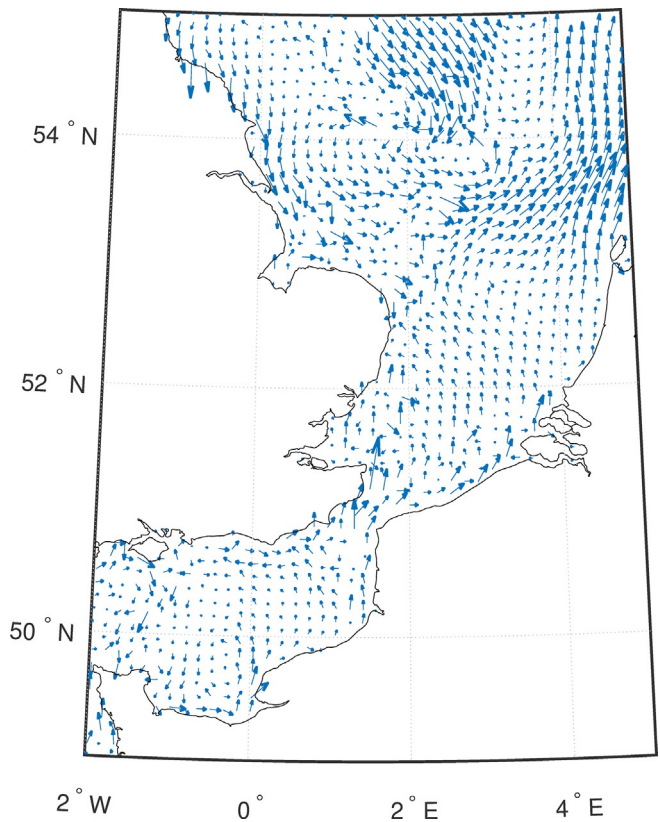

Fig. 11.6 Modeled 28-day average surface currents in the southern North Sea. Subsampled from the tide only 1.5 km NEMO environmental prediction model, run for 1 month (December 2013).

4.1 Turbulent mixing and the flushing of coastal seas

Due to the shallow nature of the continental shelf, the frictional influence of the sea bed on the tidal flow can extend to the surface. The vertically sheared current profile causes varying levels of tidal mixing through the water column. At the same time seasonal surface heating can stratify shelf seas, enabling baroclinic tides (MacKinnon and Gregg, 2003) to be generated internally within the water column. When a vertically uniform horizontal flow interacts with a changing topography (such as the shelf edge) this disturbance of the isotherms and isopycnals generates an internal tide. At the coast freshwater plumes also contribute to the density differences. The structure of the water column at the coast is primarily a balance between buoyancy inputs and turbulent mixing, mainly as a result of the barotropic tide (Simpson and Hunter, 1974). Current shear generates turbulence, which causes vertical mixing (Simpson et al., 1996), and a bottom roughness, which can result in the time-varying resuspension and transport of material from the bed or the formation of bed forms, such as dunes and ripples (e.g., Davies and Robins, 2017). Wind (Simpson and Bowers, 1981) and wave (Jones and Monismith, 2008) stresses at the surface contribute to the mixing of surface properties into the water column, while waves can also interact with the near bed current boundary layer enhancing the resuspension and sediment transport processes (Malarkey and Davies, 2012). The generation of internal tides along boundary layers within shelf seas, also act to vertically mix the water column as the internal waves generate turbulence as they propagate and break (Palmer et al., 2008; MacKinnon and Gregg, 2003; Rippeth and Inall, 2002). In shelf seas, tides may have a significant impact on weather (Arnold et al., 2021) due to the mixing of seasonal stratification influencing sea surface temperatures and in turn wind speeds and precipitation.

In shallow water, the transport of water and the properties it is carrying are rarely symmetric during each phase of the tide (flood and ebb), due to tidal asymmetries, and interactions with wind forcing, waves and other baroclinic circulations. Over a tidal cycle, the net movement is known as the residual circulation. Tidal flushing (Cook, 1982) is the systematic replacement of water (and the material it carries) in a coastal region due to the tidal flow. The flushing rate, r, is related to the intertidal volume (known as the tidal prism, P) and the low tide volume, V, by $r = P/(P + V)$. Alongside the flushing time, residence time and age are quantities used to describe the rate of water exchange. Phelps et al. (2013) demonstrate how these parameters

are used to describe the rate of offshore freshwater transport and basin replenishment in a region of freshwater influence (ROFI).

4.2 Transport of properties and materials

At the land sea interface, the transport of matter often requires management. The examples presented below cover some key issues: sediment transport, pollution, and salt intrusion.

Sediment transport is initiated when the critical bed shear stress for the particles in the seabed composition is reached. The sediment then moves along the bed or becomes suspended into the water column (van Rijn, 1993). Mixed sediments create sheltering effects (sand and gravel) and cohesion (mud) complicates the movement (see McCarron et al., 2019 and Lichtman et al., 2018, respectively). In coastal locations sediment transport is often the result of interactions between waves and currents and the resultant bottom boundary layer. Once the sediment is mobile, bed forms of different sizes such as ripples, dunes, and sand bars can form. Ripples are small features (relative to the water depth) that can result due to the oscillatory flow under a sea surface wind wave or a continuous current flow. Steep ripples, that form under surface wind waves, can complicate the transport processes through the creation of turbulent vortices, which enhance the suspended sediment concentration and can lift it higher into the water column to be transported by the current (Malarkey and Davies, 2004). Under very fast flow regimes these bed form features can be "washed out" creating a sheet-flow sediment transport regime in the immediate vicinity of the bed (Malarkey et al., 2009).

Once eroded from the bed, sediments are transported in the direction of the flow at the depth they are positioned in the water column. In regions of freshwater influence (ROFIs), the water column structure over the tidal cycle and density driven circulation also influence the net transport of sediments (Brown et al., 2015). The flow may be oscillatory due to wave effects but over both the wave and/or tidal period a net transport will often result due to shallow water effects causing asymmetries in the transport (e.g., Barnard et al., 2013). When the flow slows to below the critical shear threshold the sediment will either settle toward or become stationary on the bed. Where suspended sediment is deposited will depend on whether it reaches the bed before the current velocity increases again (Souza and Lane, 2013). As sediments pass through the water column they experience both changing current velocities and wave effects. In regions that stratify sediments can become trapped in different layers of the water column. An example of

sediment trapping is the formation of a turbidity maximum within an estuary at the edge of the salt wedge, which moves position with the excursion of the tides (Asp et al., 2018).

The movement of sediment around our coasts leads to areas of erosion and deposition. Where there are communities and infrastructure at the coast, changing beach levels and navigation channels require careful management to avoid hazardous impacts. Where human intervention occurs, for example, use of groynes and dredging, the feedbacks will be observed both locally and down drift of the change. This is why the concepts of sediment budgets and Littoral Cells have been developed for coastal management (Cooper and Pontee, 2006). These approaches help map the source, pathway, and sink of sediments and, more recently, quantify the sediment fluxes. In the past sediment cells were thought of as being closed systems, very often between headlands, and focused on the barotropic tidal circulation with consideration of intermittent storm driven circulation. Now it is appreciated that headland bypassing can occur due to wave activity (Valiente et al., 2020) and that baroclinic processes can cause sediments of different grain size to follow different transport pathways within the same cell (Brown et al., 2015). By identifying transport pathways and budgets, one can enable the longer-term, wide reaching impacts of human intervention to be better understood, thereby limiting the adverse consequences (e.g., beach starvation and harbor siltation) of new management activities by working with natural processes.

It is not only natural biogeochemical and physical properties whose transport pathways are influenced by the tide. At the land-sea interface anthropogenic contaminants, pollution, and waste (debris) enter the shelf sea system through land run-off, ground water, and industrial activity. Contaminants include, for example, metals (potentially radionuclides) from industrial waste, and organic matter such as sewage, pesticides, fertilizers, polychlorinated biphenyls (PCBs), or petroleum hydrocarbons from oil spills. The transport of anthropogenic biogeochemicals influences the quality of coastal ecosystems and habitats, making it critical to identify the sources of coastal pollution to manage them appropriately (Tosic et al., 2018). The particles or dissolved substances can be traced by monitoring or modeling the dynamics of the freshwater plume (e.g., Hunt and Jones, 2020). These particles can bind to sediments or form suspended particles themselves. When they settle, they often become trapped in sediment sinks such as nearshore sand and mud flats or in saltmarshes (e.g., Croudace et al., 2019). With rising sea levels and changing wave and surge conditions the potential for historically buried contaminated sediments becoming eroded

and re-released into the environment is of increasing concern. Coastal landfill sites are also exposed to the same hazards (Beaven et al., 2020). The mixing and replenishment or dilution of the water column properties thus play a key role in sustaining healthy coastal ecosystems that support food webs and habitats, which in turn support carbon capture and storage (Nordhaus et al., 2018). In shallow waters, the tide is a key contributor to the circulation, mixing, and offshore transport of anthropogenic matter that is brought into the coastal system though land-sea water fluxes.

Tide-driven salt-intrusion is another potential hazard at the coast, impacting availability of freshwater for agriculture and drinking. Salt intrusion is identified as a serious problem in many estuaries, including the Saint Lawrence estuary (Matte et al., 2014), the Pearl River (Payo-Payo et al., 2022), and Ganges-Brahmaputra-Meghna (GBM) delta (Bricheno et al., 2021). In these and other estuaries, the tides generate strong mixing bringing salt water up rivers with salt-intrusion reaching 100s of km inland. Salt intrusion length is defined as the upstream horizontal distance of a specific isohaline (e.g., 0.5 PSU) from the estuarine mouth. At short timescales the tidal mixing and advection dominate changes in river salinity. For example, in the GBM delta, tidally driven changes in local salinity can be as large as 10 PSU during a 12.4-h semi-diurnal cycle (Bricheno et al., 2021).

5. Tidal observations at the coast

Historically, the measurement of tides has been undertaken using instruments known as tide gauges. Despite the nomenclature, these systems are capable of measuring all types of sea-level variability, but their use has become synonymous with their original purpose of tidal measurement and the term 'tide gauge' has perpetuated.

5.1 Tide gauge networks

Since their early use was driven by a need to understand tidal fluctuations for safe navigation, tide gauges were often deployed locally by port authorities. During the 19th century, for instance, the Mersey Docks & Harbour Board established an impressive network of 12 sea-level monitoring stations along the Mersey in North West England. Nowadays, national and international networks of tide gauges have been established alongside these local networks, to monitor a variety of coastal hazards, including tides, storm surges, tsunamis, and the long-term trends in sea-level that are associated with climate change. These coordinated 'multihazard' systems sometimes

developed in response to some natural disaster, for example, the UK network of over 40 tide gauges arose following the 1953 North Sea storm surge, when Northerly winds associated with a low-pressure system caused extensive flooding and around 2400 deaths in the UK, the Netherlands and at sea (Baxter, 2005). More recently, the Sumatra tsunami of 2004 led to the development of dedicated networks of tsunami warning tide gauges in the Indian Ocean, northeast Atlantic, Mediterranean and Caribbean regions. In the Pacific Ocean, where the risk of a tsunami is relatively high, large monitoring networks are in place. For instance, in Japan, 190 tide gauges are operated by a variety of organizations, including 72 that fall under the remit of the Japanese Meteorological Agency. The US National Oceanic and Atmospheric Administration (NOAA) oversees a network of over 200 tide gauges that evolved from the US Coast Survey's tide gauge installations in the 19th Century.

Globally, the activity of such national and regional networks is coordinated through the Intergovernmental Oceanographic Commission's Global Sea Level Observing System (GLOSS, https://www.gloss-sealevel.org/), of which the GLOSS Core Network (Fig. 11.7) is a key component (IOC, 2012). This is a global collection of almost 300 high quality tide gauge stations that can satisfy a full range of research requirements. Most notably, the collective data has formed the scientific basis for the Intergovernmental Panel on Climate Change (IPCC) reports on long-term sea-level change (IPCC WG1, 2021). Historically, the global distribution of tide gauges

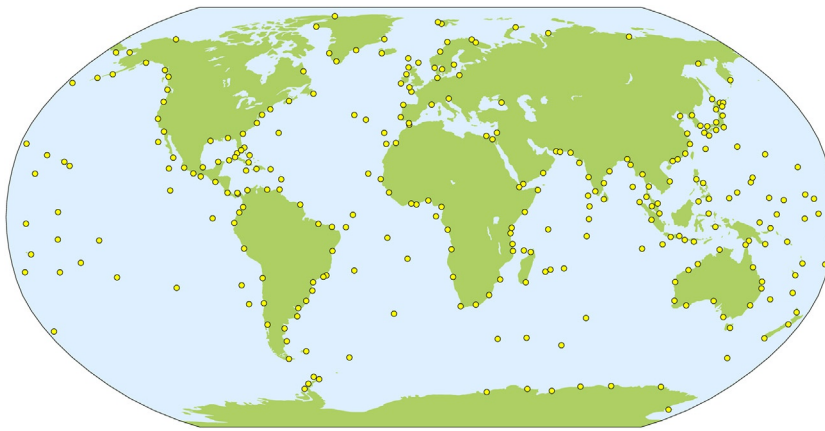

Fig. 11.7 The locations of the GLOSS Core Network of tide gauge stations. *(©Andy Matthews, Permanent Service for Mean Sea Level, National Oceanography Centre.)*

has been biased toward the Northern Hemisphere where sea-level monitoring is long-established, but as Fig. 11.7 shows, the GLOSS Core Network has been selected to be globally representative, as far as possible. GLOSS also coordinates the dissemination of tide gauge data and related land motion datasets via dedicated international data centers, such as the Permanent Service for Mean Sea Level (PSMSL) and the Système d'Observations du Niveau des Eaux Littorales (SONEL).

5.2 Measurement technology

The earliest tide gauges, such as the nilometers used by the Ancient Egyptians on the River Nile, consisted of a graduated marker from which the level of the sea surface could be judged by eye at regular intervals and then recorded. Some nilometers consisted of vertical corridors lined with steps, which led down to the river, but most early tide gauges were simpler affairs and were akin to a vertical ruler mounted on or cut into a harbor wall. These are still in use today and are generally referred to as tide boards or tide staffs. The zero level of these early tide gauges would be measured relative to some nearby benchmark on land, so that a record of sea-level relative to land would emerge over time. During the 19th Century, such labor-intensive practices gave way to mechanical instruments known as self-registering float gauges, which became the tide gauge standard for the next 100 years or so (Woodworth, 2015). These consisted of a large vertical tube (the stilling well) that was fixed to a sea wall or similar, with an opening to the sea. The stilling well removed much of the wave action and contained a float that would rise and fall with the tide, its movements being recorded on a paper chart on a clock-driven chart recorder by a pen that was connected to the float via a pulley system. Some float and stilling well gauges are still in use today, including the National Oceanography Centre's tide gauge at the Ukrainian base of Vernadsky, Antarctica. Remarkably, despite the hostile polar environment, a float gauge has been in operation there for over 60 years.

Nevertheless, most modern tide gauges are of two types: either underwater pressure transducers (which measure sea-level height from the hydrostatic pressure of the overlying water column) or above-water systems such as radar or acoustic sensors. Above-water instruments emit radar or acoustic pulses and detect the reflected signal to determine the distance to the sea surface. In recent years, radar-based systems (Fig. 11.8) have proven more popular as acoustic gauges must be mounted within temperature-controlled

Fig. 11.8 A radar tide gauge and tide board at Ganters Bay, St Lucia. *(©Jeff Pugh, National Oceanography Centre.)*

sounding tubes due to the dependence of the speed of sound upon air temperature. Above-surface systems are undoubtedly cheap and easy to maintain, but they can become damaged by shipping or over-topped by extreme wave conditions. The opposite is true for underwater systems, so the most resilient tide gauges often harness two technologies in parallel.

Comprehensive guidance relating to the use of different tide gauge technologies is provided by the Intergovernmental Oceanographic Commission (IOC) Manuals on Sea Level Measurement and Interpretation, the most recent of which (Volume V) relates to the use of radar technology (IOC, 2016).

Whichever technology solution is used, GLOSS standards emphasize that it is essential to establish the height of the measuring point of the tide gauge sensor relative to a collection of at least 5 nearby benchmarks (BMs),

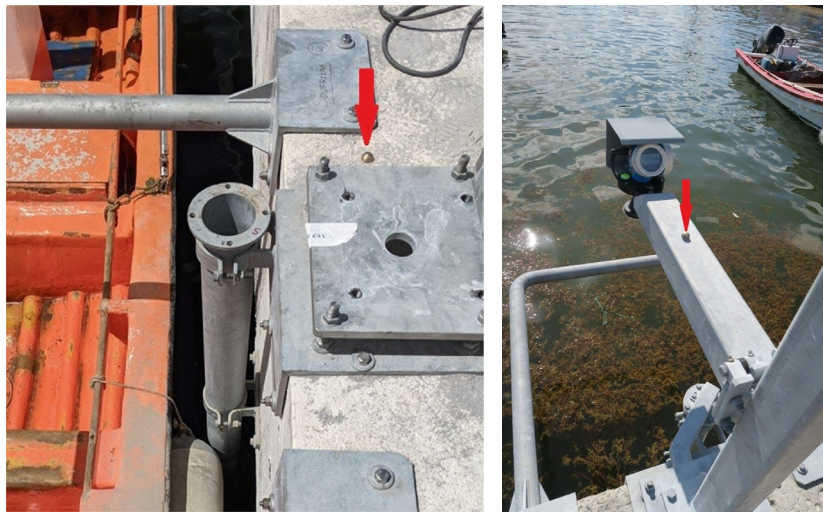

Fig. 11.9 Tide Gauge Bench Marks (TGBM) at the base and on the supporting arm of a radar tide gauge. *(©Jeff Pugh, National Oceanography Centre.)*

which are fixed at stable points on land. BMs are land level reference points that generally take the form of a brass bolt set into a horizontal solid rock surface such as a quayside (Fig. 11.9), although they can also be represented by cut marks in vertical walls. A Tide Gauge Bench Mark (TGBM) is installed, if possible, in hard rock as close as possible to the tide gauge. This on or alongside the tide gauge equipment forms the primary BM and its purpose is twofold: Firstly, it allows sea-level observations to be reported relative to a known point on land, which preserves the continuity of a tide gauge record if, for example, instruments are changed or relocated. Secondly, the height of a TGBM can be measured periodically relative to the heights of other the nearby benchmarks via levelling exercises, to monitor any change in land levels surrounding the tide gauge. The local levelling is important to establish local stability or not.

To facilitate the precise measurement of vertical land movement at tide gauges, global navigation satellite system (GNSS) receivers have increasingly been co-located with tide gauges. These receivers measure changes in land elevation by the detection of positioning and timing information from a constellation of navigational satellites such as GPS (USA), GLONASS (Russia), BeiDou (China) and GALILEO (Europe). Ideally, a GNSS BM should be located close to the supporting structure (usually referred to as

the GNSS monument) and levelled to the TGBM (Woodworth et al., 2017). This is not only important for ensuring stability in the local area, but enables the TGBM to be located in a geocentric reference frame, so that it becomes more easily comparable with satellite altimetry data. Over the last decade, it has become apparent that 'multipath' GNSS signals reflected off the sea surface can themselves be used to infer sea-level height (e.g., Larson et al., 2013) and this emerging technology, known as GNSS interferometric reflectometry (GNSS-IR) may lead to GNSS receivers becoming a standalone tide gauge system in the future (Fig. 11.10).

Modern tide gauges tend to sample sea level at regular intervals of between 1 s and several minutes, depending upon their primary purpose. Tide gauges that are used for early warning purposes, say for tsunami monitoring, require very high frequency sampling and rapid transmission of data

Fig. 11.10 GNSS-based tide gauge at Sheerness, UK. *(©David Jones, National Oceanography Centre.)*

in near real time to national and international hazard warning centers. Consequently, these gauges employ fast telecommunication methods for data transmission. Fixed or mobile phone lines are a popular telemetry choice for tide gauges, but for very remote areas, such as polar regions, satellite-based communications systems are often adopted. Whichever telemetry method is used, the data are generally stored locally on a data collection platform (known as a data logger) and then transmitted to the data owner. In some cases, if data are not required urgently, a telemetry system may not be necessary and the data can be stored locally on the data logger for extended periods and downloaded periodically on visits to the tide gauge site.

Despite advances in tide gauge technology, most modern tide gauges still encompass a tide board or staff (Fig. 11.8), to serve as a visual check on the more sophisticated technology and are a common feature in many ports and harbors.

5.3 Data types

As described in Section 5.1, tide gauge networks are operated for a variety of purposes. Some are used by port authorities in real time for navigation purpose, while others are used by national and regional coastal hazard monitoring agencies for early detection of extreme sea-level events such as storm surges and tsunamis. Fast delivery of data (within several minutes) is needed for these purposes and there is little opportunity for extensive quality control, so data are often provided in a raw, unchecked format. These are generally referred to as near real-time data.

Where tide gauge data are used for scientific purposes, such as validating numerical models, evaluating sea-level extremes and assessing long-term trends associated with climate change, data must first be scrutinized, quality-checked, and any anomalies flagged to potential users. These data, referred to as delayed mode, are usually assembled into longer series, for example, annual files and are embargoed for a short period until checks are complete.

In practice many tide gauge networks are used for multiple purposes and both near real-time and delayed mode data streams exist for the same tide gauge stations, so users must ensure that the data stream is fit for their chosen purpose. Fortunately, there are a number of international data centers with responsibility for collating and distributing different types of sea-level data. These centers operate under the auspices of the (IOC's) GLOSS and their

differing roles are described to potential users on the dedicated webpage https://gloss-sealevel.org/data.

5.4 Quality control and data analysis

While tide gauges are designed to afford high quality accurate observations of sea level, erroneous data can arise due to factors such as instrumental failures, shipping collisions, storm damage and general wear and tear. Therefore, it is essential to ensure that tide gauge data are consistent and to make any errors apparent to the user, so that they can draw robust conclusions from the dataset. This is achieved through the application of rigorous quality control procedures to a tide gauge record, often via a purpose-built computer-based software package that allows visual inspection of the data and identification and earmarking of suspect data points. Newer packages include some statistical tools and algorithms to automatically detect suspicious data, reducing the need for manual intervention, while some tide gauge operators (e.g., Puertos del Estado, Spain) have harnessed this technology to quality control observations in near real time.

A fundamental part of quality control is the use of a technique known as tidal analysis, which separates the tidal component of a tide gauge record from the nontidal effects, thus allowing the operator to more easily identify errors, particularly smaller ones, which can be masked by tidal changes, especially in locations that experience a large tidal range. Full procedural recommendations for the quality control of sea-level data are too numerous to be described here, but the interested reader can refer to UNESCO/IOC's Manual on Quality Control of in situ Sea Level Observations (UNESCO/IOC, 2020) for a comprehensive overview. This manual describes the strict quality control standards that are applied to tide gauge data from the GLOSS Core Network and which must also be implemented for other tide gauge records to be assimilated into the archives of those GLOSS data centers that accepted quality-controlled sea-level data: the Permanent Service for Mean Sea Level, the University of Hawaii Sea Level Center and the British Oceanographic Data Centre. Such rigorous quality control demands a level of skill that is not widespread among tide gauge operators, which means that many tide gauge records never reach the archives of these GLOSS data centers and the datasets therefore become lost to the scientific community. It is hoped that the increasing automation of quality control procedures might halt the loss of these datasets in the future.

Operators of tide gauges, or other interested parties can make use of the guidelines available in the Ocean Best Practices System (OBPS), which is

operated under the auspices of the IOC (https://www.oceanbestpractices.org/). This is a community driven repository to record and distribute methodologies, manuals and other technical documentation, to ensure consistency of collection, processing, and storage.

5.5 Sea-level rise (SLR), climate assessments and storm surges

As mentioned in Section 5.1, tide gauge records are often used by scientists in regular research assessments of the global changes in sea level that are believed to be associated with a warming climate. These assessments are based on tide gauge records and sea-level measurements from space by satellite altimetry (Stammer and Cazenave, 2017). The most well-known of these are the assessments of the Intergovernmental Panel on Climate Change (IPCC), which were first produced in 1990, the latest (AR6 working group 1 report) were produced in August 2021 for COP26, with the full report due in 2022. AR6 concluded that global mean sea level (GMSL) rose by an average of 1.3 mm year^{-1} between 1901 and 1971 and accelerated thereafter to 1.9 mm year^{-1} between 1971 and 2006, reaching 3.7 mm year^{-1} between 2006 and 2018 (IPCC, 2021). Of these changes, roughly 50% has been ascribed to thermal expansion of the oceans, while another 43% is attributed to the melting of land-based ice sheets and glaciers and the remainder is due to changes in water storage on land. IPCC assessments do not just evaluate historic data, but they also use climate models to make a range of future projections of sea-level rise (SLR). These models look at the impact of shared socioeconomic pathway (SSP) scenarios, which are based upon different combinations of future greenhouse gas emissions, pollution controls, and socioeconomic assumptions. For a very high emissions scenario (SSP5–8.5), AR6 suggests GMSL is likely to rise by an average of 0.77 m by 2100, while a very low emissions scenario (SSP1–1.9) indicates a likely average SLR of 0.38 m by 2100.

An obvious implication of SLR is that the probability of coastal flooding is likely to increase, therefore, reliable estimates will be needed to plan coastal protection (Woodworth et al., 2021). It is important to unpick the combination of gradually rising Mean Sea Level (MSL) from warming-related changes in the frequency and intensity of storm surges that might increase this probability further. The IPCC's AR6 has suggested that the proportion of tropical cyclones that are intense has increased over the past 40 years and that this is likely to continue, but the total number of tropical cyclones is likely to remain unchanged. In addition, compound flooding due to storm surges, rainfall, and/or river flow has increased over the last

century, and this is set to continue. However, this is primarily due to SLR increasing extreme water levels (Menéndez and Woodworth, 2010) rather than changes in storm surge frequency and intensity. It should be noted that there is higher uncertainty in the predictions of changes in future storminess, while the projections of mean SLR are better bound.

5.6 Acceleration of SLR and SLR modulating tidal constituents

With SLR, water depth will increase, and change how tidal energy can penetrate especially in shallow water areas. Numerous observational studies have used tide gauge data to show significant trends in tidal range at many locations around the world, comparable in magnitude to the rate of SLR at some locations (Haigh et al., 2020 and references therein).

A number of recent modeling studies have suggested changes in tidal range resulting from future changes in mean sea level, see for example Pickering et al. (2012), Pickering et al. (2017), Ward et al. (2012), Pelling et al. (2013), and Wilmes et al. (2017). This is because increased sea level will reduce friction and move basins toward or away from resonance. These modeling studies all suggest that changes in tidal range will be of the order of plus or minus 10% of any changes in mean sea level, with large spatial variability. Although small in comparison to the mean sea level changes, altered tidal ranges could enhance (or reduce) coastal flooding at some locations. Fig. 11.11 shows a model projection for future tides (by 2050) on the North West European continental shelf, caused by a spatially nonuniform SLR of 0.1–0.3 m. Consequently, this causes a mixture of increases and decreases in tidal range by over 0.06 m. Increases in tidal range on the shelf, can be further amplified into river channels. Modeling studies in tide-dominated deltas, for example, De Dominicis et al. (2020) predict tidal

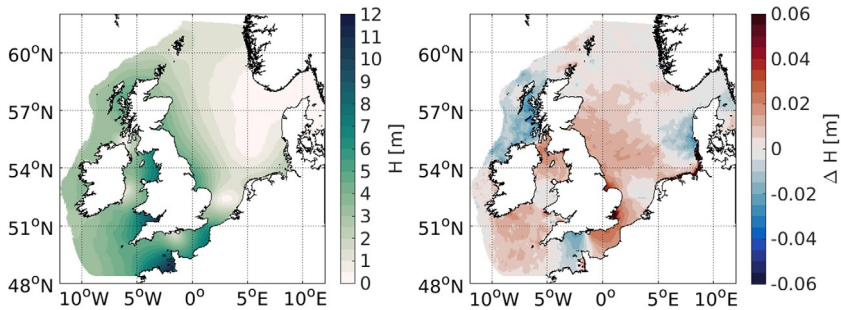

Fig. 11.11 Spring peak tidal range during present (left) and absolute change due to future climate conditions (right) based on De Dominicis et al. (2018).

amplification in the Pearl River Delta due to SLR. Similar findings are reported in the Yangtze (Gong et al., 2012), Ganges Brahmaputra-Meghna delta (Bricheno et al., 2016), and in the Mekong (Nhan, 2016).

6. Tidal applications

While the tide-producing force of the Earth-Moon-Sun system is predictable, as we have seen in Chapter 4, the tides that we observe at the coasts are distorted by factors such as ocean bathymetry, the effects of the Earth's rotation and the presence of land masses. As a result, tides can vary dramatically from one place to the next. Shallower coastal regions generally have larger tidal ranges than those of the open ocean, primarily due to local resonance. Some coasts like those of North East Australia including the Gulf of Carpentaria experience large diurnal tides, while others have semi-diurnal tides, in some cases with tidal ranges that exceed 12 m (such as in the Severn Estuary, UK, and the Bay of Fundy, Canada). In very shallow water, tides can become so distorted that multiple tides can be observed per day, such as the double high water feature that is observed at Southampton, UK.

Given the variety of tidal regimes and tidal ranges that occur globally, the need to forecast tidal patterns to facilitate port and harbor operations and to provide advance warning of coastal flooding has been long-established, going back as far as the Ancient Egyptians and their use of nilometers to identify the onset of flooding on the River Nile.

6.1 Predictions for ports and harbors

Tidal predictions have conventionally been published as tables of times and heights of high and low waters (Fig. 11.12) for selected locations, which allow port authorities and vessel operators to safely navigate coastal waters at appropriate times. Timings of high and low waters are usually given in hours and minutes, while heights are in meters relative to some known datum (Section 6.2) at a given location. The use of tide tables extends back as far as the 18th Century, when Richard and George Holden first produced useful printed tables for the port of Liverpool, in North West England, based on the method proposed by Daniel Bernoulli (Cartwright, 1999; Woodworth, 2002), but nowadays they are more likely to be distributed via the internet or using mobile phone applications.

For ports which have good quality and long tide gauge records (Standard or Reference ports), tidal predictions are generally prepared from sets of harmonic constituents that have been calculated from harmonic analysis of an

LIVERPOOL (GLADSTONE DOCK)

UT(GMT) **Datum : Chart Datum** **Year : 2022**

January

	Time	m		Time	m
1 Sa	0357	1.81	**16** Su	0426	2.58
	0930	9.06		1018	8.48
	1622	1.83		1658	2.43
	2156	9.21		2236	8.45
2 Su A	0452	1.54	**17** M C	0504	2.37
	1023	9.41		1054	8.73
	1719	1.45		1737	2.18
	2250	9.44		2313	8.63
3 M	0544	1.36	**18** Tu	0541	2.18
	1113	9.66		1129	8.91
	1814	1.16		1815	1.99
	2342	9.53		2348	8.75
4 Tu	0633	1.31	**19** W	0617	2.04
	1203	9.78		1203	9.02
	1906	1.03		1852	1.86
5 W	0032	9.46	**20** Th	0021	8.82
	0721	1.40		0654	1.95
	1251	9.75		1236	9.08
	1955	1.07		1930	1.79
6 Th	0121	9.25	**21** F	0055	8.83
	0807	1.63		0730	1.94
	1339	9.57		1310	9.06
	2043	1.30		2006	1.81
7 F	0208	8.91	**22** Sa	0131	8.77
	0853	1.98		0807	2.02
	1425	9.26		1345	8.99
	2129	1.67		2042	1.92
8 Sa	0255	8.51	**23** Su	0209	8.64
	0938	2.39		0844	2.18
	1512	8.88		1423	8.85
	2215	2.12		2120	2.09
9 Su B	0344	8.09	**24** M	0250	8.45
	1026	2.82		0923	2.40
	1603	8.45		1505	8.67
	2303	2.57		2200	2.32
10 M	0438	7.72	**25** Tu D	0336	8.22
	1120	3.19		1009	2.66
	1658	8.04		1554	8.43
	2357	2.95		2249	2.56
11 Tu	0539	7.46	**26** W	0433	7.98
	1223	3.43		1105	2.91
	1802	7.74		1656	8.17
				2353	2.78
12 W	0057	3.17	**27** Th	0543	7.82
	0648	7.39		1218	3.04
	1330	3.47		1812	8.01
	1910	7.63			
13 Th	0200	3.19	**28** F	0114	2.81
	0754	7.54		0702	7.89
	1433	3.31		1344	2.91
	2015	7.73		1935	8.09
14 F	0256	3.05	**29** Sa	0233	2.59
	0851	7.84		0815	8.22
	1528	3.03		1503	2.52
	2110	7.96		2048	8.41
15 Sa	0344	2.82	**30** Su	0341	2.21
	0937	8.17		0920	8.69
	1615	2.72		1613	1.99
	2157	8.22		2152	8.82
			31 M	0442	1.80
				1016	9.17
				1715	1.46
				2247	9.18

February

	Time	m		Time	m
1 Tu A	0536	1.46	**16** W C	0527	2.05
	1107	9.56		1112	8.95
	1809	1.03		1801	1.70
	2336	9.41		2329	8.88
2 W	0625	1.23	**17** Th	0604	1.75
	1154	9.80		1145	9.18
	1858	0.78		1839	1.44
3 Th	0022	9.46	**18** F	0002	9.07
	0710	1.16		0641	1.53
	1238	9.86		1217	9.34
	1942	0.77		1914	1.28
4 F	0104	9.35	**19** Sa	0035	9.17
	0751	1.27		0717	1.42
	1319	9.74		1251	9.41
	2022	0.99		1949	1.26
5 Sa	0143	9.09	**20** Su	0109	9.17
	0829	1.56		0751	1.45
	1358	9.46		1324	9.37
	2059	1.41		2022	1.39
6 Su	0221	8.74	**21** M	0145	9.05
	0904	1.97		0825	1.62
	1436	9.06		1400	9.23
	2133	1.93		2055	1.65
7 M	0258	8.33	**22** Tu	0223	8.82
	0939	2.46		0900	1.91
	1517	8.57		1439	8.96
	2207	2.49		2130	2.01
8 Tu B	0340	7.88	**23** W D	0306	8.49
	1018	2.98		0941	2.29
	1603	8.03		1525	8.56
	2247	3.02		2215	2.46
9 W	0431	7.44	**24** Th	0359	8.07
	1109	3.45		1034	2.72
	1700	7.50		1626	8.05
	2342	3.47		2316	2.92
10 Th	0539	7.10	**25** F	0511	7.68
	1224	3.75		1149	3.06
	1815	7.15		1752	7.65
11 F	0100	3.68	**26** Sa	0048	3.16
	0702	7.06		0642	7.60
	1348	3.70		1329	3.04
	1938	7.16		1928	7.68
12 Sa	0215	3.56	**27** Su	0221	2.94
	0819	7.34		0806	7.94
	1458	3.35		1458	2.57
	2048	7.47		2049	8.11
13 Su	0316	3.21	**28** M	0334	2.43
	0916	7.79		0915	8.51
	1555	2.89		1612	1.92
	2139	7.89		2151	8.65
14 M	0406	2.81			
	1000	8.25			
	1642	2.43			
	2221	8.29			
15 Tu	0448	2.41			
	1037	8.64			
	1723	2.03			
	2256	8.62			

Computed and formatted by POLTIPS-3 ; the National Oceanography Centre's Tidal Software

Fig. 11.12 A tide table for Liverpool, produced by the National Oceanography Centre.

existing tide gauge record (Pugh and Woodworth, 2014). The process of prediction is essentially the reverse of harmonic analysis and generates time series of tidal heights for each location. Consequently, tide tables for these Reference or Standard ports are often set out to show hourly tidal heights each day. Since the harmonic constituents for a given location varies little over a few decades, these tables can be produced several years in advance.

However, there are many other ports for which long observational tidal datasets do not exist, but where tidal predictions are still needed. For these Secondary or Subordinate stations, simplified information is given in the form of local time and height differences for high and low waters, relative to those at a nearby Standard or Reference Port. These differences can be calculated from observational tidal records at the Secondary station of as little as 1 month. Recently developed global tide models are also available, from which one can calculate the tide anywhere (Byrne et al., 2021; Lyard et al., 2021).

6.2 Tidal datums

Tide tables specify tidal heights relative to a vertical reference level called the datum and the most commonly used is Chart Datum (CD), which usually approximates the lowest tide level that is likely to occur under normal meteorological conditions (the Lowest Astronomical Tide, LAT). This means that tidal heights will almost always be presented as positive values in tide tables.

However, Chart Datum is unique to a location and cannot be used in comparisons of tidal heights at different ports. Instead, a national datum is often defined, to which all other heights can be related. In the past, this was commonly established by measuring Mean Sea Level (MSL) at a particular location over an extended period of time (nominally the lunar nodal period of 18.6 years) and then transferring this reference level to other locations via levelling. Ordnance Datum (Newlyn) or ODN is the national datum for most of the UK and is defined as the average value of sea level recorded at Newlyn between 1915 and 1921.

Other tidal datums are used to define a certain phase of the tide and these are established by taking sea-level averages during these phases over a number of years. Commonly used datums, include Mean High Water (MHW) and Mean Low Water (MLW), which are the average values for high water and low water, respectively, over a specific period and Mean Tide Level (MTL), which is the average of the two. Mean High Water Springs

(MHWS) denotes the average spring tide high water level, while Mean Low Water Springs (MLWS) equates to the average spring low water level.

6.3 Predictions for flood forecasting

The regular and predictable pattern of the tides is altered by weather effects, as the combined effects of low atmospheric pressure and wind stress cause the sea surface to dome upwards, in what is known as a storm surge. Since the speed of tidal propagation increases in deeper water and bottom friction is simultaneously reduced in deep water, a storm surge event leads to faster propagation of the tide than would be predicted by tide tables. This is particularly problematic when a storm surge coincides with high water as the risk of flooding is increased and alternative methods of forecasting are needed. This was illustrated in January 1953 when low atmospheric pressure and northerly winds led to the development of a storm surge of up to 3 m in the North Sea that coincided with high tides, causing extensive flooding and 307 deaths on the east coast of the England and 1800 in the Netherlands. Consequently, many national flood defense agencies now operate flood warning systems that integrate near real-time tide gauge observations, with forecasts from numerical tide-surge models. These models combine tidal and meteorological forcings, to mimic the interactions between the tide and surge in order to better predict the arrival time and heights of the resulting peak water levels and the forecasts are validated with tide gauge observations. In the UK, tide-surge models are run in real time by the Met Office. Their results are transmitted to the Environment Agency and used alongside data from the National Tide Gauge Network for coastal flood warning in England and Wales.

6.4 Tidal power

The movement of the tides around coastlines represents a significant and largely untapped energy resource. Tidal power comes in two main forms, tidal stream (which harnesses the kinetic energy of the tidal current) and tidal range (which harnesses potential energy from the change in sea level).

Electricity generation from tidal range is a very well understood, but little used resource because of its high initial cost. Technologies that harness tidal range energy include barrages, lagoons and tidal reefs. They involve the construction of a dam (similar to large-scale hydroelectric power schemes) in order to create a difference in the head between the two bodies of water either side of the dam wall as water flows in and out of the estuary. Once

the desired difference in head is reached, sluice gates are opened and water is released through turbines generating electricity.

Energy generation from tidal stream/current is a much newer concept that harnesses the horizontal movement of water, which accompanies the rise and fall of the tides. Tidal stream energy can be captured by an underwater turbine, in much the same way as wind energy is harnessed with a wind turbine. However, due to the density of the water, tidal stream turbines can produce 800–900 times the power of a wind turbine of the same size, rotating at the same speed (Jahromi et al., 2011). Tidal stream turbines can be sited individually or as part of a tidal array, made up of several turbines. The turbines can be attached to the seabed or hang into the water from a floating structure.

An advantage of tidal energy over other renewable resources is that it is highly predictable, however, it produces an intermittent source of energy. Due to the phases of the tides, peak energy production would not occur at the same time every day. There is also variation in the energy produced due to the spring-neap tidal cycle, with maximum power output on a neap tide being about half that output on a spring tide (Yates et al., 2013).

There have been suggestions that the intermittency of tidal range generation could be overcome through the conjunctive operation of multiple barrages along a coastline (Burrows et al., 2009), or in a lagoon, using multiple cells from which the water is released through the turbines sequentially. Another option is to use tidal power in conjunction with battery storage.

6.5 Summary

Though generated in deep water, it is at the coast where most people interact with tides. We measure them, use their energy, and experience their impacts. It is at the coast that the tides become interactive with humans and shapes our shorline. Interactions with other processes: storms, waves, and rivers can modulate the tide, leading to changes in its phase and amplitude. When it meets the coast, a 'well behaved' deep water tide becomes amplified and constrained, leading to fast flows around headlands. Tidal flows at the coast impact the health of the seas through mixing and flushing, and represent an underused resource for renewable energy. It is at the coast that we most readily observe tides, and where measurements have been made for 1000s of years. A network of tide gauges is vital for safe navigation, the observations are used in harmonic analysis to enable tidal prediction and to validate numerical models used for future forecasting. When well curated,

data from these observations and can give early warning of extreme water level events, and provide evidence of long-term trends in sea levels associated with climate change.

Acknowledgments

The Centre for Environment, Fisheries and Aquaculture Science (CEFAS) are thanked for providing access to the WaveNet service that has maintained an operational wave buoy in Liverpool Bay since 2002. The National Tide and Sea Level Facility (NTSLF) are thanked for the provision of the Liverpool Gladstone Dock tide gauge record through the British Oceanographic Data Centre (BODC).

References

Ardhuin, F., Roland, A., Dumas, F., Bennis, A.-C., Sentchev, A., Forget, P., Wolf, J., Girard, F., Osuna, P., Benoit, M., 2012. Numerical wave modeling in conditions with strong currents: dissipation, refraction and relative wind. J. Phys. Oceanogr. 42 (12), 2101–2120.

Arnold, A.K., Lewis, H.W., Hyder, P., Siddorn, J., O'Dea, E., 2021. The sensitivity of british weather to ocean tides. Geophys. Res. Lett. 48 (3), e2020GL090732.

Asp, N.E., Gomes, V.J.C., Schettini, C.A.F., Souza-Filho, P.W.M., Siegle, E., Ogston, A.S., Nittrouer, C.A., Silva, J.N.S., Nascimento, W.R., Souza, S.R., Pereira, L.C.C., Queiroz, M.C., 2018. Sediment dynamics of a tropical tide-dominated estuary: turbidity maximum, mangroves and the role of the Amazon River sediment load. Estuar. Coast. Shelf Sci. 214, 10–24.

Barnard, P.L., Erikson, L.H., Elias, E.P.L., Dartnell, P., 2013. Sediment transport patterns in the San Francisco Bay Coastal System from cross-validation of bedform asymmetry and modeled residual flux. Mar. Geol. 345, 72–95.

Baxter, P.J., 2005. The east coast big flood, 31 January–1 February 1953: a summary of the human disaster. Phil. Trans. R. Soc. A 363, 1293–1312.

Beaven, R.P., Stringfellow, A.M., Nicholls, R.J., Haigh, I.D., Kebede, A.S., Watts, J., 2020. Future challenges of coastal landfills exacerbated by sea level rise. Waste Manag. 105, 92–101.

Bell, P.S., 2010. Submerged dunes and breakwater embayments mapped using wave inversions of shore-mounted marine X-band radar data. In: IEEE International Geoscience and Remote Sensing Symposium, Honolulu, HI, pp. 4334–4337, https://doi.org/10.1109/IGARSS.2010.5652634.

Bolaños, R., Osuna, P., Wolf, J., Sanchez-Arcilla, A., 2011. Development of the POLCOMS-WAM current-wave model. Ocean Model. 36 (1–2), 102–115.

Bolaños, R., Brown, J., Souza, A., 2014. Wave-current interactions in a tide dominated estuary. Cont. Shelf Res. 87, 109–123.

Bricheno, L.M., Wolf, J., Islam, S., 2016. Tidal intrusion within a mega delta: an unstructured grid modelling approach. Estuar. Coast. Shelf Sci. 182, 12–26.

Bricheno, L.M., Wolf, J., Sun, Y., 2021. Saline intrusion in the Ganges-Brahmaputra-Meghna megadelta. Estuar. Coast. Shelf Sci. 252, 107246.

Brown, J.M., Davies, A.G., 2009. Methods for medium-term prediction of the net sediment transport by waves and currents in complex coastal regions. Cont. Shelf Res. 29 (11 – 12), 1502–1514.

Brown, J., Wolf, J., 2009. Coupled wave and surge modelling for the eastern Irish Sea and implications for model wind-stress. Cont. Shelf Res. 29 (10), 1329–1342.
Brown, J., Bolanos-Sanchez, R., Souza, A., 2014. Controls on monthly estuarine residuals: Eulerian circulation and elevation. Ocean Dyn. 64 (4), 587–609.
Brown, J.M., Amoudry, L.O., Souza, A.J., Rees, J., 2015. Fate and pathways of dredged estuarine sediment spoil in response to variable sediment size and baroclinic coastal circulation. J. Environ. Manag. 149, 209–221.
Brown, J., Yelland, M.J., Pascal, R.W., Jones, D.S., Balfour, C.A., Hargreaves, G., Martin, B., Cardwell, C.L., Pinnell, R., Bell, P.S., Pullen, T., Silva, E., Prime, T., 2020. Key WireWall project data generated during the field deployment at Hall Road Crosby (North of Liverpool UK), between October 2018 and March 2019. British Oceanographic Data Centre, National Oceanography Centre, NERC, UK, https://doi.org/10.5285/acd939f0-38e7-57b0-e053-6c86abc0aa19. https://www.bodc.ac.uk/data/published_data_library/catalogue/10.5285/acd939f0-38e7-57b0-e053-6c86abc0aa19/.
Burrows, R., Walkington, I.A., Yates, N.C., Hedges, T.S., Wolf, J., Holt, J., 2009. The tidal range energy potential of the west coast of the United Kingdom. Appl. Ocean Res. 31, 229–238.
Byrne, D., Polton, J., Bell, C., 2021. Creation of a global tide analysis dataset: application of NEMO and an offline objective analysis scheme. J. Oper. Oceanogr. https://doi.org/10.1080/1755876X.2021.2000249.
Cartwright, D.E., 1999. Tides: A Scientific History. Cambridge University Press, Cambridge. 292pp.
Cook, D.O., 1982. Tidal flushing. In: Beaches and Coastal Geology. Encyclopedia of Earth Sciences Series, Springer, New York, NY, https://doi.org/10.1007/0-387-30843-1_463.
Cooper, N.J., Pontee, N.I., 2006. Appraisal and evolution of the littoral 'sediment cell' concept in applied coastal management: experiences from England and Wales. Ocean Coast. Manag. 49 (7–8), 498–510.
Corbella, S., Stretch, D.D., 2012. Multivariate return periods of sea storms for coastal erosion risk assessment. Nat. Hazards Earth Syst. Sci. 12, 2699–2708.
Croudace, I.W., Teasdale, P.A., Cundy, A.B., 2019. 200-year industrial archaeological record preserved in an Isle of Man saltmarsh sediment sequence: geochemical and radiochronological evidence. Quat. Int. 514, 195–203.
Davidson, M.A., O'Hare, T.J., George, K.J., 2008. Tidal modulation of incident wave heights: fact or fiction? J. Coast. Res. 24 (sp2), 151–159.
Davies, A.G., Robins, P.E., 2017. Residual flow, bedforms and sediment transport in a tidal channel modelled with variable bed roughness. Geomorphology 295, 855–872.
De Dominicis, M., Wolf, J., O'Hara Murray, R., 2018. Comparative effects of climate change and tidal stream energy extraction in a shelf sea. J. Geophys. Res. Oceans 123 (7), 5041–5067.
De Dominicis, M., Wolf, J., Jevrejeva, S., Zheng, P., Hu, Z., 2020. Future interactions between sea level rise, tides, and storm surges in the world's largest urban area. Geophys. Res. Lett. 47 (4).
Esteban, M., Jamero, M.L., Nurse, L., Yamamoto, L., Takagi, H., Thao, N.D., Mikami, T., Kench, P., Onkui, M., Nellas, A., Chrichton, R., Valenzuela, V.P., Chadwick, C., Avelino, J.E., Tan, N., Shibayama, T., 2019. Adaptation to sea level rise on low coral islands: lessons from recent events. Ocean Coast. Manag. 168, 35–40.
Godin, G., 1999. The propagation of tides up rivers with special considerations on the Upper Saint Lawrence River. Estuar. Coast. Shelf Sci. 48 (3), 307–324.
Gong, Z., Zhang, C., Wan, L., Zuo, J., 2012. Tidal level response to sea-level rise in the yangtze estuary. China Ocean Eng. 26 (1), 109–122.

Gouldby, B., Wyncoll, D., Panzeri, M., Franklin, M., Hunt, T., Hames, D., Tozer, N., Hawkes, P., Dornbusch, U., Pullen, T., 2017. Multivariate extreme value modelling of sea conditions around the coast of England. Proc. Inst. Civ. Eng. Marit. Eng. 170 (1), 3–20.

Green, M.O., Coco, G., 2014. Review of wave-driven sediment resuspension and transport in estuaries. Rev. Geophys. 52 (1), 77–117.

Haigh, I.D., Pickering, M.D., Green, J.A.M., Arbic, B.K., Arns, A., Dangendorf, S., Hill, D.-F., Horsburgh, K., Howard, T., Idier, D., Jay, D.A., Jänicke, L., Lee, S.B., Müller, M., Schindelegger, M., Talke, S.A., Wilmes, S.-B., Woodworth, P.L., 2020. The tides they are a-changin': a comprehensive review of past and future nonastronomical changes in tides, their driving mechanisms and future implications. Rev. Geophys. 58 (1), e2018RG000636.

Hoitink, A.F.J., Jay, D.A., 2016. Tidal river dynamics: implications for deltas. Rev. Geophys. 54 (1), 240–272.

Horrevoets, A.C., Savenije, H.H.G., Schuurman, J.N., Graas, S., 2004. The influence of river discharge on tidal damping in alluvial estuaries. J. Hydrol. 294 (4), 213–228.

Hunt, S., Jones, H.F.E., 2020. The fate of river-borne contaminants in the marine environment: characterising regions of freshwater influence (ROFIs) and estuary plumes using idealised models and satellite images. Mar. Pollut. Bull. 156, 111169.

Idier, D., Bertin, X., Thompson, P., Pickering, M., 2019. Interactions between mean sea level, tide, surge, waves and flooding: mechanisms and contributions to sea level variations at the coast. Surv. Geophys. 40, 1603–1630.

IOC, 2012. The Global Sea Level Observing System (GLOSS) Implementation Plan—2012. UNESCO/Intergovernmental Oceanographic Commission. 37pp. (IOC Technical Series No. 100).

IOC, 2016. Manual on sea-level measurements and interpretation, volume V: Radar gauges. Intergovernmental Oceanographic Commission of UNESCO, Paris. 104pp (IOC Manuals and Guides No. 14, vol. V; JCOMM Technical report No. 89;, (English).

IPCC, 2021. Climate change 2021: the physical science basis. In: Masson-Delmotte, V., Zhai, P., Pirani, A., Connors, S.L., Péan, C., Berger, S., Zhou, B. (Eds.), Contribution of working group I to the sixth assessment report of the intergovernmental panel on climate change. Vol. 40. Cambridge University Press, pp. 1603–1630. In Press. eophysics.

Jahromi, M.J., Maswood, A.I., Tseng, K.-J., 2011. Long term prediction of tidal currents. IEEE Syst. J. 5, 146–155.

Jevrejeva, S., Bricheno, L., Brown, J., Byrne, D., De Dominicis, M., Matthews, A., Rynders, S., Palanisamy, H., Wolf, J., 2020. Quantifying processes contributing to marine hazards to inform coastal climate resilience assessments, demonstrated for the Caribbean Sea. Nat. Hazards Earth Syst. Sci. 20, 2609–2626.

Jones, N.L., Monismith, S.G., 2008. Modeling the influence of wave-enhanced turbulence in a shallow tide- and wind-driven water column. J. Geophys. Res. 113, C03009. https://doi.org/10.1029/2007JC004246.

Larson, K.M., Lofgren, J., Haas, R., 2013. Coastal sea level measurements using a single geodetic GPS receiver. Adv. Space Res. 51 (8), 1301–1310. https://doi.org/10.1016/j.asr.2012.04.017.

Leonardi, N., Kolker, A.S., Fagherazzi, S., 2015. Interplay between river discharge and tides in a delta distributary. Adv. Water Resour. 80, 69–78.

Lewis, M.J., Neill, S.P., Hashemi, M.R., Reza, M., 2014. Realistic wave conditions and their influence on quantifying the tidal stream energy resource. Appl. Energy 136, 495–508.

Lewis, M., Neill, S.P., Robins, P., Hashemi, M.R., Ward, S., 2017. Characteristics of the velocity profile at tidal-stream energy sites. Renew. Energy 114 (Part A), 258–272.

Lewis, M., Palmer, T., Hashemi, R., Robins, P., Saulter, A., Brown, J., Lewis, H., Neill, S., 2019. Wave-tide interaction modulates nearshore wave height [in special issue: topical Collection on the 15th International Workshop on Wave Hindcasting and Forecasting in Liverpool, UK, September 10–15, 2017]. Ocean Dyn. 69 (3), 367–384.
Lichtman, I.D., Baas, J.H., Laurent, A.O., Torne, P.D., Malarkey, J., Hope, J.A., Peakall, J., Paterson, D.M., Bass, S.J., Cooke, R.D., Manning, A.J., Davies, A.G., Parsons, D.R., Ye, L., 2018. Bedform migration in a mixed sand and cohesive clay intertidal environment and implications for bed material transport predictions. Geomorphology 315, 17–32.
Longuet-Higgins, M.S., 1970a. Longshore currents generated by obliquely incident sea waves, 1. J. Geophys. Res. 75 (33), 6778–6789.
Longuet-Higgins, M.S., 1970b. Longshore currents generated by obliquely incident sea waves, 2. J. Geophys. Res. 75 (33), 6790–6801.
Longuet-Higgins, M.S., Stewart, R.W., 1964. Radiation stresses in water waves; a physical discussion with applications. Deep-Sea Res. 11, 529–562.
Lyard, F.H., Allain, D.J., Cancet, M., Carrère, L., Picot, N., 2021. FES2014 global ocean tide atlas: design and performance. Ocean Sci. 17 (3), 615–649.
Lyddon, C., Brow, J.M., Leonardi, N., Plater, A.J., 2018. Uncertainty in estuarine extreme water level predictions due to surge-tide interaction. PLoS One 13 (10), e0206200.
MacKinnon, J.A., Gregg, M.C., 2003. Mixing on the late-summer New England shelf–solibores, shear and stratification. J. Phys. Oceanogr. 33, 1476–1492.
Malarkey, J., Davies, A.G., 2004. An eddy viscosity formulation for oscillatory flow over vortex ripples. J. Geophys. Res. 109, C12016.
Malarkey, J., Davies, A.G., 2012. A simple procedure for calculating the mean and maximum bed stress under wave and current conditions for rough turbulent flow based on Soulsby and Clarke's (2005) method. Comput. Geosci. 43, 101–107.
Malarkey, J., Pan, S., Li, M., O'Donoghue, T., Davies, A.G., O'Connor, B.A., 2009. Modelling and observation of oscillatory sheet-flow sediment transport. Ocean Eng. 36 (11), 873–890.
Matte, P., Secretan, Y., Morin, J., 2014. Temporal and spatial variability of tidal-fluvial dynamics in the St. Lawrence fluvial estuary: an application of nonstationary tidal harmonic analysis. J. Geophys. Res. Oceans 119 (9), 5724–5744.
McCarron, C.J., Van Landeghem, K.J.J., Baas, J.H., Amoudry, L.O., Malarkey, J., 2019. The hiding-exposure effect revisited: a method to calculate the mobility of bimodal sediment mixtures. Mar. Geol. 410, 22–31.
Menéndez, M., Woodworth, P.L., 2010. Changes in extreme high water levels based on a quasi-global tide-gauge dataset. J. Geophys. Res. 115, C10011.
Nhan, H.N., 2016. Tidal regime deformation by sea level rise along the coast of the Mekong delta. Estuar. Coast. Shelf Sci. 183, 382–391.
Nordhaus, I., Roelke, D.L., Vaquer-Sunyer, R., Winter, C., 2018. Coastal systems in transition: from a 'natural' to an 'anthropogenically-modified' state. Estuar. Coast. Shelf Sci. 211, 1–5.
Osuna, P., Monbaliu, J., 2004. Wave–current interaction in the Southern North Sea. J. Mar. Syst. 52 (1–4), 65–87.
Palmer, M.R., Rippeth, T.P., Simpson, J.H., 2008. An investigation of internal mixing in a seasonally stratified shelf sea. J. Geophys. Res. 113 (C12), C12005.
Payo-Payo, M., Bricheno, L.M., Dijkstra, Y.M., Cheng, W., Gong, W., Amoudry, L.O., 2022. Multiscale temporal response of salt intrusion to transient river and ocean forcing. J. Geophys. Res. Oceans 127, e2021JC017523.
Pelling, H.E., Mattias Green, J.A., Ward, S.L., 2013. Modelling tides and sea level rise: to flood or not to flood. Ocean Model. 63, 21–29.

Phelps, J.J.C., Polton, J.A., Souza, A.J., Robinson, L.A., 2013. Hydrodynamic timescales in a hyper-tidal region of freshwater influence. Cont. Shelf Res. 63, 13–22.
Pickering, M.D., Wells, N.C., Horsburgh, K.J., Green, J.A.M., 2012. The impact of future sea-level rise on the European shelf tides. Cont. Shelf Res. 35, 1–15.
Pickering, M.D., Horsburgh, K.J., Blundell, J.R., Hirschi, J.J.-.M., Nicholls, R.J., Verlaan, M., Wells, N.C., 2017. The impact of future sea-level rise on the global tides. Cont. Shelf Res. 142, 50–68.
Prandle, D., 2003. Relationships between tidal dynamics and bathymetry in strongly convergent estuaries. J. Phys. Oceanogr. 33 (12), 2738–2750.
Pugh, D., Woodworth, P., 2014. Sea-level science: understanding tides, surges, tsunamis and mean sea-level changes. Cambridge University Press, Cambridge. https://doi.org/10.1017/CBO9781139235778.
Pugh, D.T., Woodworth, P.L., Wijeratne, E.M.S., 2020. Seiches around the Shetland Islands. Pure Appl. Geophys. 177 (2), 591–620.
Ray, R.D., Foster, G., 2016. Future nuisance flooding at Boston caused by astronomical tides alone. Earth's Future 4.
Rippeth, T.P., Inall, M.E., 2002. Observations of the internal tide and associated mixing across the Malin shelf. J. Geophys. Res. 107 (C4), 3028. https://doi.org/10.1029/2000JC000761.
Salvadori, G., Durante, F., Tomasicchio, G.R., D'Alessandro, F., 2015. Practical guidelines for the multivariate assessment of the structural risk in coastal and off-shore engineering. Coast. Eng. 95, 77–83.
Sassi, M.G., Hoitink, A.J.F., 2013. River flow controls on tides and tide-mean water level profiles in a tidal freshwater river. Journal of Geophysical Research: Oceans 118 (9), 4139–4151.
Scott, T., Masselink, G., Russell, P., 2011. Morphodynamic characteristics and classification of beaches in England and Wales. Mar. Geol. 286 (1–4), 1–20.
Simpson, J.H., Bowers, D., 1981. Models of stratification and frontal movement in shelf seas. Deep Sea Res. Part A 28, 727–738. https://doi.org/10.1016/0198-0149(81)90132-1.
Simpson, J.H., Hunter, J.R., 1974. Fronts in the Irish Sea. Nature 250, 404–406. https://doi.org/10.1038/250404a0.
Simpson, J.H., Sharples, J., Rippeth, T.P., 1991. A prescriptive model of stratification induced by freshwater runoff. Estuar. Coast. Shelf Sci. 33 (1), 23–35.
Simpson, J.H., Crawford, R.W., Rippeth, T.P., Campbell, A.R., Choek, J.V.S., 1996. The vertical structure of turbulent dissipation in shelf seas. J. Phys. Oceanogr. 26, 1579–1590.
Souza, A.J., Lane, A., 2013. Effects of freshwater inflow on sediment transport. J. Oper. Oceanogr. 6 (1), 27–31.
Stammer, D., Cazenave, A. (Eds.), 2017. Satellite Altimetry Over Oceans and Land Surfaces. CRC Press, Boca Raton. 617pp.
Tosic, M., Restrepo, J.D., Izquierdo, A., Lonin, S., Martins, F., Escobar, R., 2018. An integrated approach for the assessment of land-based pollution loads in the coastal zone. Estuar. Coast. Shelf Sci. 211, 217–226.
UNESCO/IOC, 2020. Quality Control of in situ Sea Level Observations: A Review and Progress towards Automated Quality Control. vol. 1 UNESCO, Paris. IOC Manuals and Guides No. 83. IOC/2020/MG/83 Vol. 1 https://unesdoc.unesco.org/ark:/48223/pf0000373566.
Valiente, G.V., Masselink, G., McCarroll, R.J., Scott, T., Conley, D., King, E., 2020. Nearshore sediment pathways and potential sediment budgets in embayed settings over a multi-annual timescale. Mar. Geol. 427, 106270.
van Rijn, L.C., 1993. Principles of Sediment Transport in Rivers, Estuaries and Coastal seas. Aqua Publications, Amsterdam, The Netherlands. 633pp.

Vilibić, I., Rabinovich, A.B., Anderson, E.J., 2021. Special issue on the global perspective on meteotsunami science: editorial. Nat. Hazards 106, 1087–1104.
Wadey, M.P., Brown, J.M., Haigh, I.D., Dolphin, T., Wisse, P., 2015. Assessment and comparison of extreme sea levels and waves during the 2013/14 storm season in two UK coastal regions. Nat. Hazards Earth Syst. Sci. 15 (10), 2209–2225.
Ward, S., Green, J.A.M., Pelling, H., 2012. Tides, sea-level sea level rise and tidal power extraction on the European shelf. Ocean Dyn. 62 (8), 1153–1167.
Wilmes, S.-.B., Green, J.A.M., Gomez, N., Rippeth, T.P., Lau, H., 2017. Global tidal impacts of large-scale ice-sheet collapses. J. Geophys. Res. Oceans 122, 8354–8370.
Wolf, J., Prandle, D., 1999. Some observations of wave–current interaction. Coast. Eng. 37 (3–4), 471–485.
Woodworth, P.L., 2002. Three Georges and one Richard Holden: the Liverpool tide table makers. Trans. Hist. Soc. Lancashire Cheshire 151, 19–51.
Woodworth, P.L., 2015. Tidal measurement. In: Monmonier, M. (Ed.), The History of Cartography: Cartography in the Twentieth Century, first ed. vol. 6. University of Chicago, Chicago, pp. 1525–1528.
Woodworth, P.L., Wöppelmann, G., Marcos, M., Gravelle, M., Bingley, R.M., 2017. Why we must tie satellite positioning to tide gauge data. EOS Trans. Am. Geophys. Union 98 (4), 13–15. https://eos.org/opinions/why-we-must-tie-satellite-positioning-to-tide-gauge-data.
Woodworth, P.L., Hunter, J.R., Marcos, M., Hughes, C.W., 2021. Towards reliable global allowances for sea level rise. Glob. Planet. Chang. 203, 103522.
Xie, D., Zou, Q.-P., Mignone, A., MacRae, J.D., 2019. Coastal flooding from wave overtopping and sea level rise adaptation in the northeastern USA. Coast. Eng. 150, 39–58.
Yates, N., Walkington, I., Burrows, R., Wolf, J., 2013. Appraising the extractable tidal energy resource of the UK's western coastal waters. Phil. Trans. R. Soc. A 371, 20120181.
Zou, Q.-P., Chen, Y., Cluckie, I., Hewston, R., Pan, S., Peng, Z., Reeve, D., 2013. Ensemble prediction of coastal flood risk arising from overtopping by linking meteorological, ocean, coastal and surf zone models. Quarterly Journal of the Royal Meteorological Society 139 (671), 298–313.